1. Studies of signal and background separation using Mann-Whitney U test

In this section, we study different jet substructure variables and compare their ability to separate the signal and background for different detector cell sizes using the Mann-Whitney U test.

By the definition of the Mann-Whitney U test, if the value of U is close to 0.5, it means that the signal and background distributions have almost identical shapes, i.e. the separation power of the variable is bad. On the other hand, if the U value is close to 0, it means that the distributions of the signal and the background are very different from each other and the separation power of the variable is great.

Figure 6 shows the representative sample of the distributions for τ_{21},τ_{32}, in different detector sizes with their corresponding U value. In τ_{21}, the separation power is better when the detector size is smaller. However, the separation power of tau32 does not improve when the detector size gets smaller.

Figure 7 shows the summary plots of the clustering in Mann-Whitney U test for the three different variables. In τ_{21}, 5 TeV has the better separation power when the detector size is smaller. However, there is not much improvement in higher energy collisions. In τ_{32}, 5 TeV has also better separation power on smaller detector size but higher energy collisions seem to have better separation power when the detector size is bigger. The $c_2^{(1)}$ does not seem to have any significant improvement in its separation power as the detector size gets smaller for all energy collision. Nevertheless, the U values of the $c_2^{(1)}$ are better than theτ_{21} and τ_{32}. In conclusion, the $c_2^{(1)}$ variable is the best parameter as its separation power is better than the other variable and does not have a significant improvement in higher energy collision.

Figure 8 shows the summary plots of the rawhit cut at 0.5 GeV in Mann Whitney U test for the three different variables. In τ_{21}, 5 and 10 TeV have better separation power on smaller detector sizes. However, there is no significant improvement in the separation power of higher energy collisions. The τ_{32} does not have any significant improvement in its separation power as the detector size gets smaller for all energy collision. Lastly, there is a slight improvement in separation power for 5, 10, and 20 TeV energy collision in $c_2^{(1)}$. At 40 TeV, no significant improvement is observed. In conclusion, the $c_2^{(1)}$ variable is the best parameter as it has the best separation power at 40 TeV energy collision than the other variables.

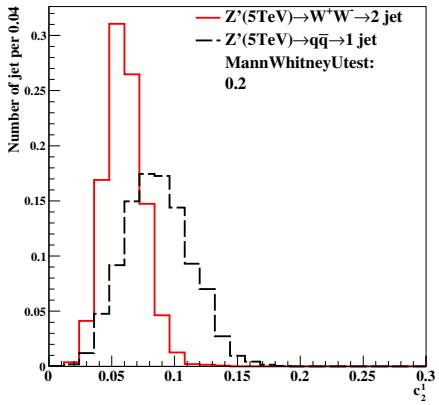

(a) 5TeV at 20×20(cm×cm) in cluster

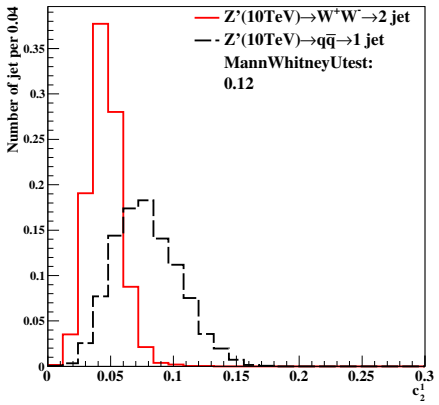

(b) 10TeV at 20×20(cm×cm) in cluster

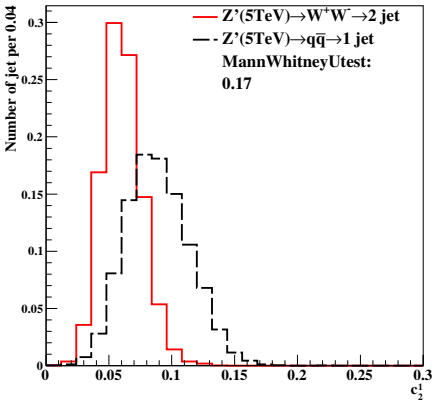

(c) 5TeV at 5×5(cm×cm) in cluster

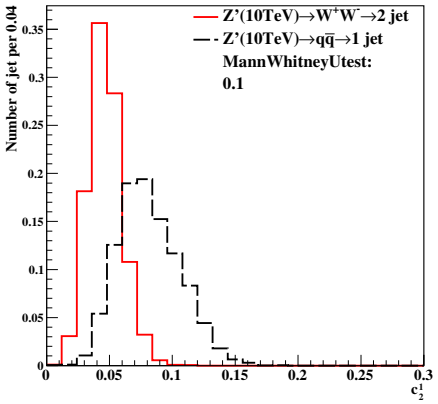

(d) 10TeV at 5×5(cm×cm) in cluster

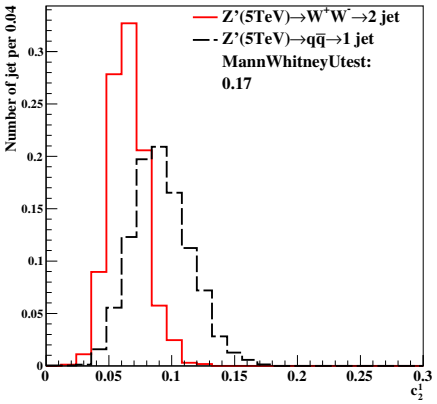

(e) 5TeV at 1×1(cm×cm) in cluster

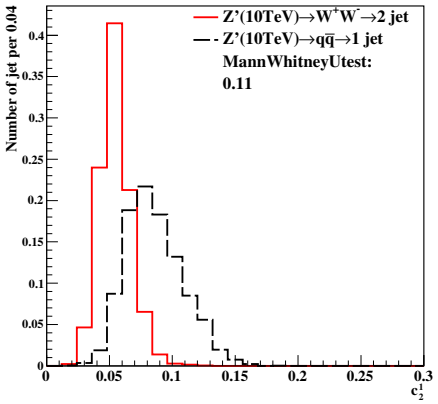

(f) 10TeV at 1×1(cm×cm) in cluster

Figure 1: Distributions of Mann-Whitney value U in 5,10TeV energy collision for $c_2^{(1)}$ in different detector sizes. Cell Size in 20×20, 5×5, and 1×1(cm×cm) are shown here.

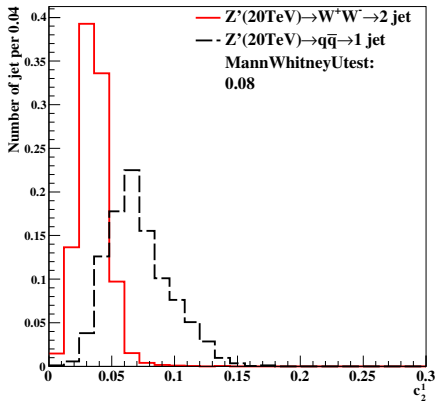

(a) 20TeV at 20×20(cm×cm) in cluster

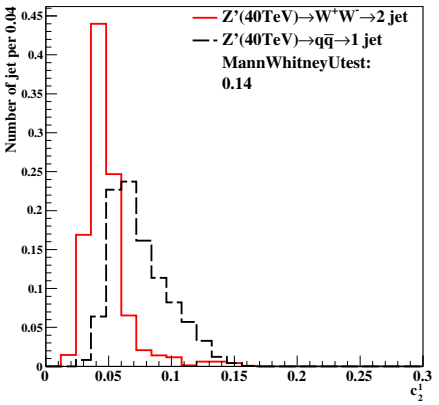

(b) 40TeV at 20×20(cm×cm) in cluster

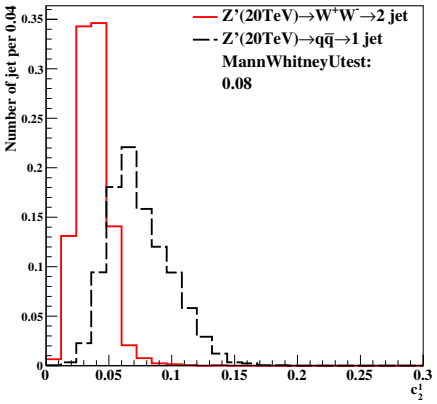

(c) 20TeV at 5×5(cm×cm) in cluster

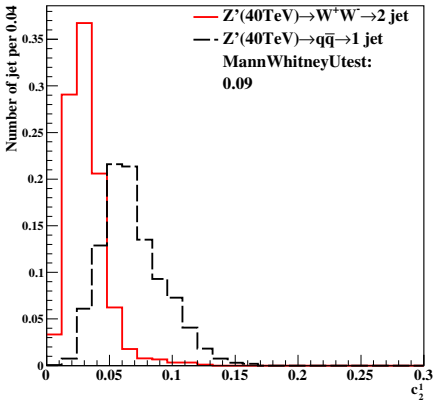

(d) 40TeV at 5×5(cm×cm) in cluster

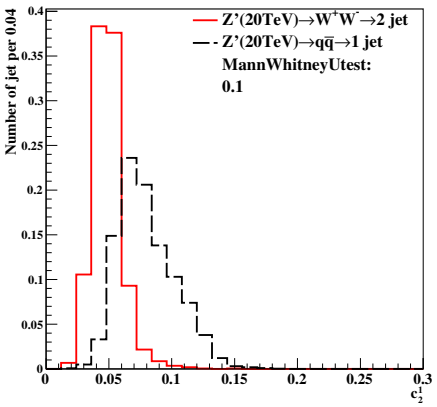

(e) 20TeV at 1×1(cm×cm) in cluster

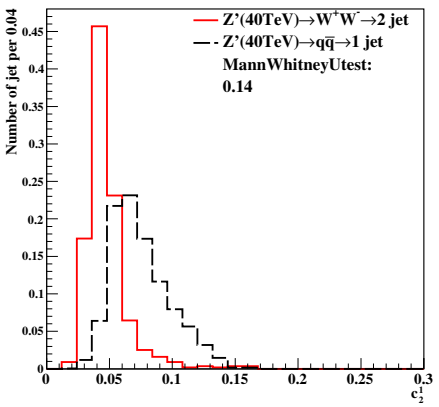

(f) 40TeV at 1×1(cm×cm) in cluster

Figure 2: Distributions of Mann-Whitney value U in 20,40TeV energy collision for $c_2^{(1)}$ in different detector sizes. Cell Size in 20×20, 5×5, and 1×1(cm×cm) are shown here.

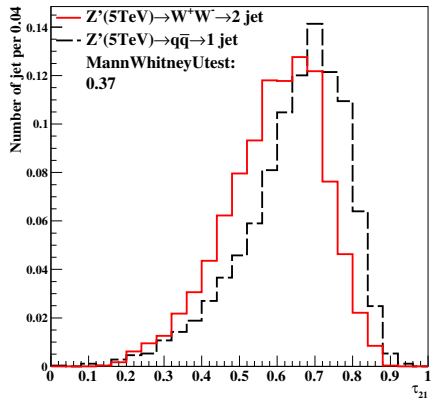

(a) 5TeV at 20×20(cm×cm) in cluster

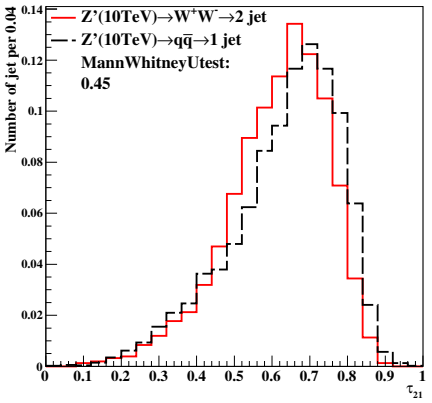

(b) 10TeV at 20×20(cm×cm) in cluster

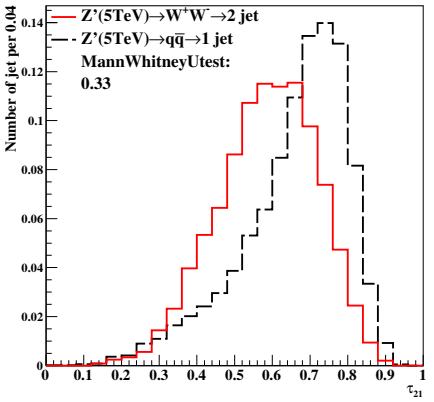

(c) 5TeV at 5×5(cm×cm) in cluster

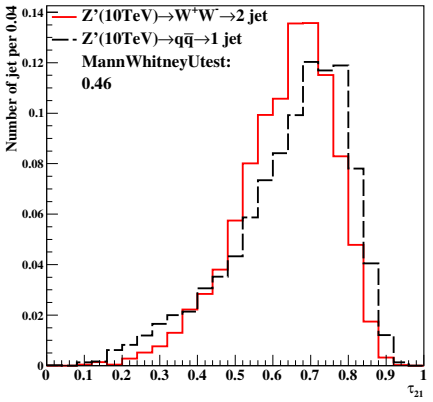

(d) 10TeV at 5×5(cm×cm) in cluster

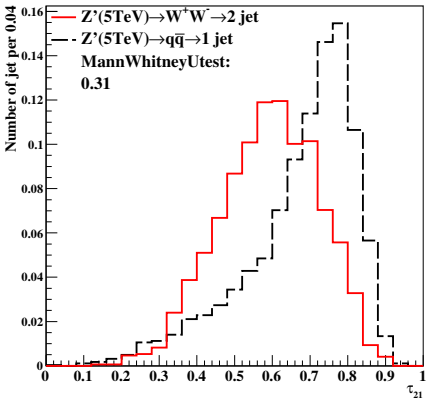

(e) 5TeV at 1×1(cm×cm) in cluster

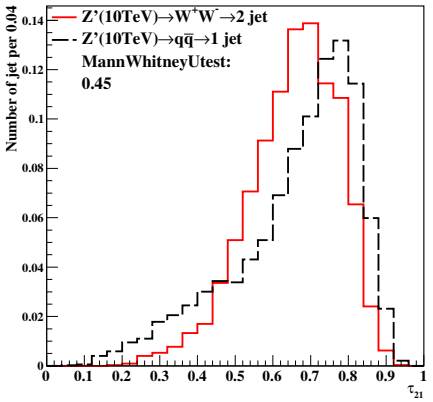

(f) 10TeV at 1×1(cm×cm) in cluster

Figure 3: Distributions of Mann-Whitney value U in 5,10TeV energy collision for τ_{21} in different detector sizes. Cell Size in 20×20, 5×5, and 1×1(cm×cm) are shown here.

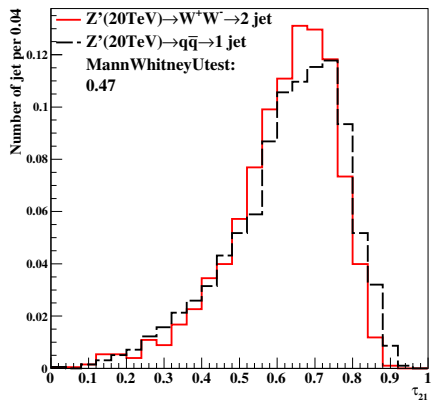

(a) 20TeV at 20×20(cm×cm) in cluster

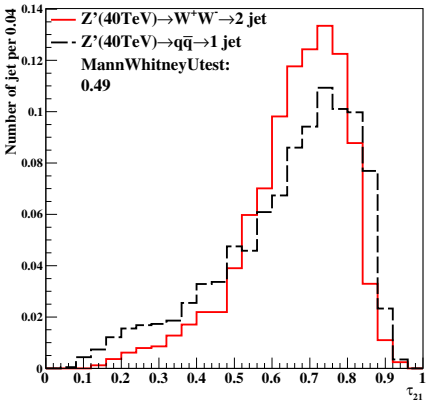

(b) 40TeV at 20×20(cm×cm) in cluster

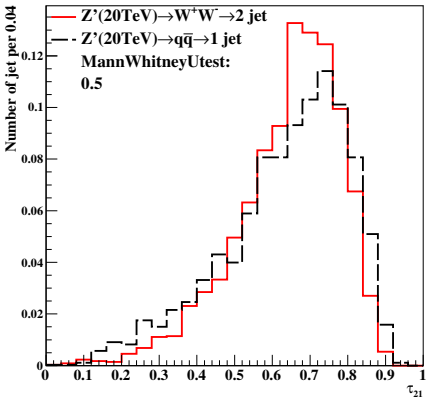

(c) 20TeV at 5×5(cm×cm) in cluster

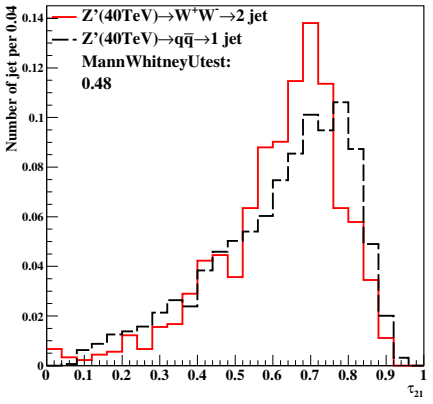

(d) 40TeV at 5×5(cm×cm) in cluster

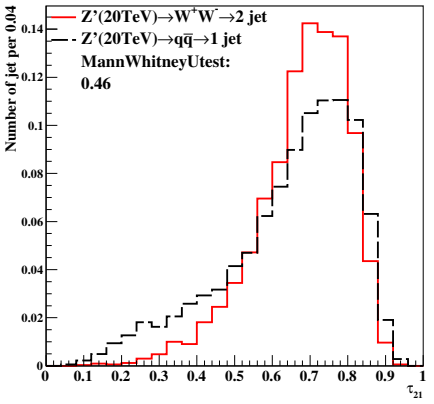

(e) 20TeV at 1×1(cm×cm) in cluster

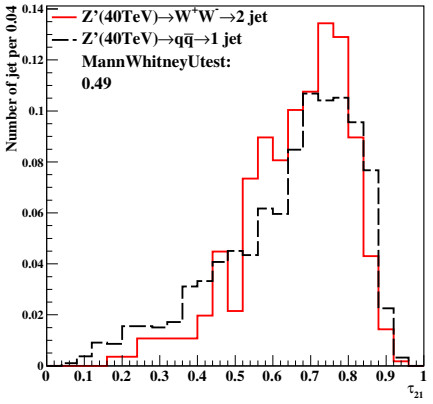

(f) 40TeV at 1×1(cm×cm) in cluster

Figure 4: Distributions of Mann-Whitney value U in 20,40TeV energy collision for τ_{21} in different detector sizes. Cell Size in 20×20, 5×5, and 1×1(cm×cm) are shown here.

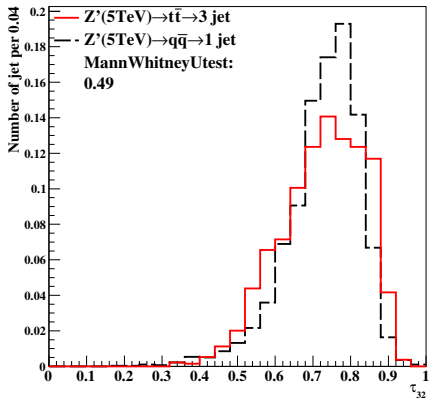

(a) 5TeV at 20×20(cm×cm) in cluster

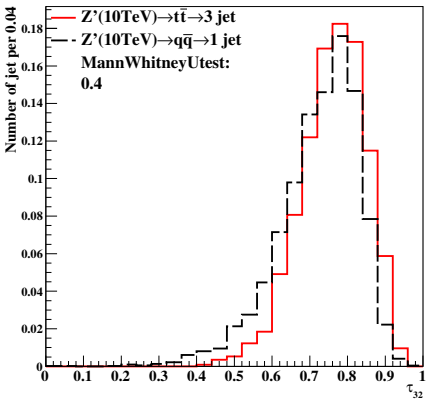

(b) 10TeV at 20×20(cm×cm) in cluster

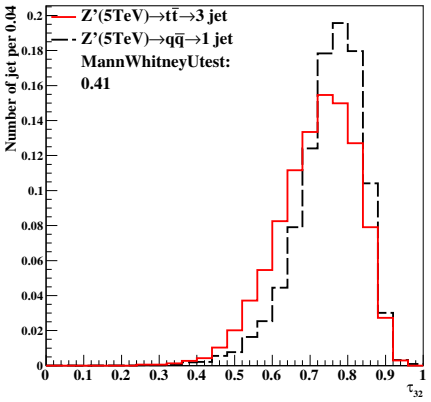

(c) 5TeV at 5×5(cm×cm) in cluster

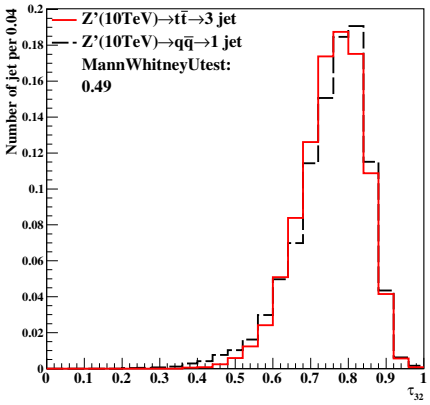

(d) 10TeV at 5×5(cm×cm) in cluster

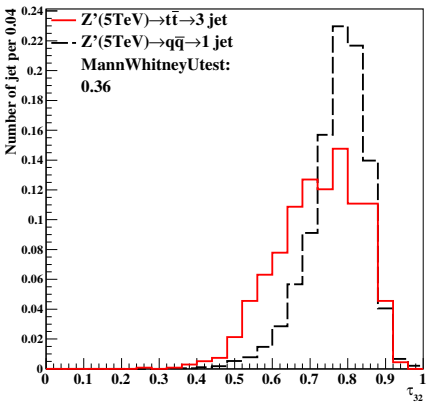

(e) 5TeV at 1×1(cm×cm) in cluster

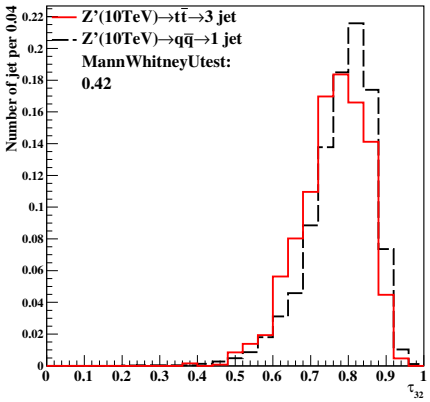

(f) 10TeV at 1×1(cm×cm) in cluster

Figure 5: Distributions of Mann-Whitney value U in 5,10TeV energy collision for τ_{32} in different detector sizes. Cell Size in 20×20, 5×5, and 1×1(cm×cm) are shown here.

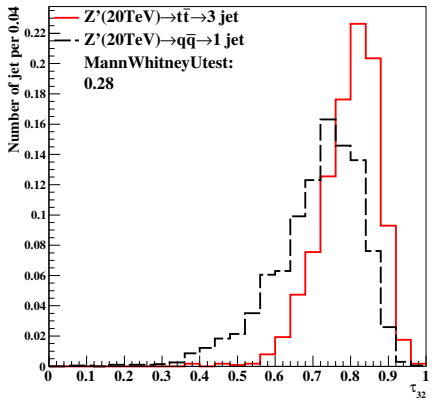

(a) 20TeV at 20×20(cm×cm) in cluster

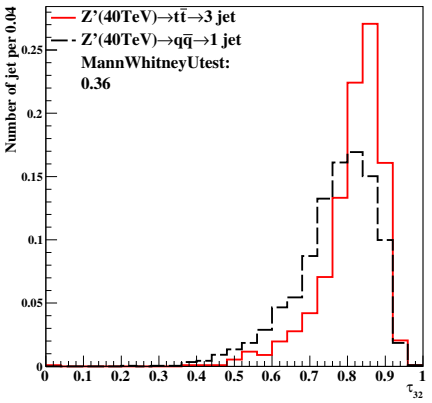

(b) 40TeV at 20×20(cm×cm) in cluster

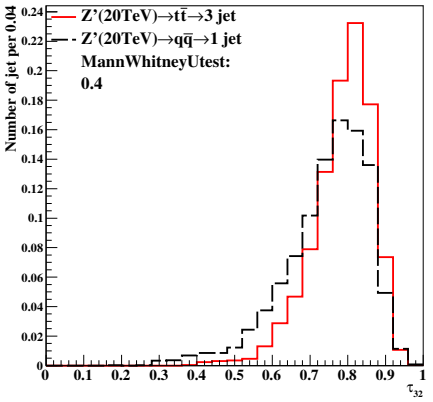

(c) 20TeV at 5×5(cm×cm) in cluster

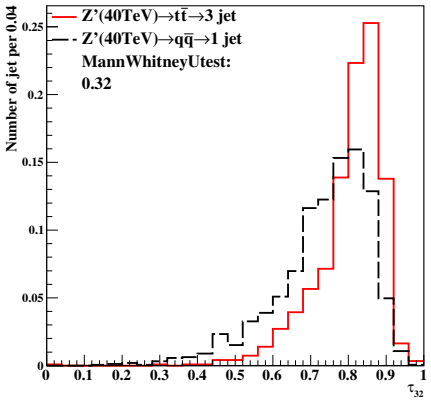

(d) 40TeV at 5×5(cm×cm) in cluster

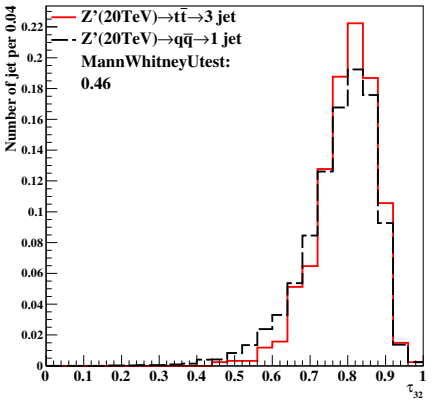

(e) 20TeV at 1×1(cm×cm) in cluster

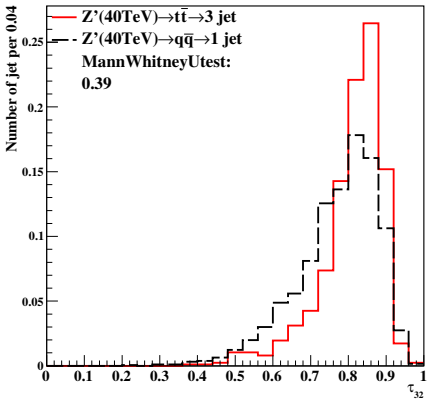

(f) 40TeV at 1×1(cm×cm) in cluster

Figure 6: Distributions of Mann-Whitney value U in 20,40TeV energy collision for τ_{32} in different detector sizes. Cell Size in 20×20, 5×5, and 1×1(cm×cm) are shown here.

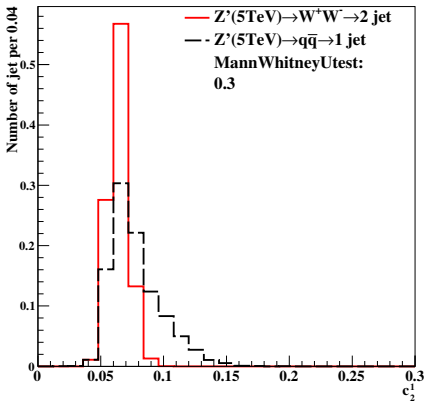

(a) 5TeV at 20×20(cm×cm) cut at 0.5GeV

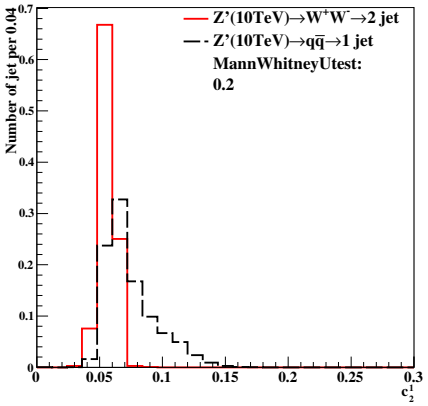

(b) 10TeV at 20×20(cm×cm) cut at 0.5GeV

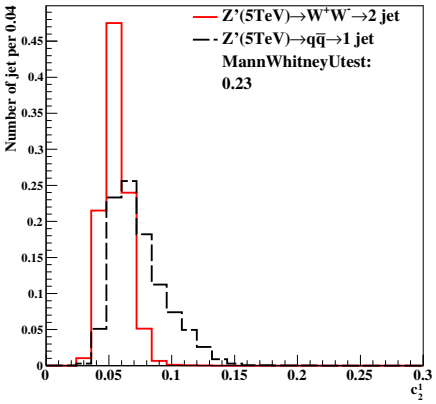

(c) 5TeV at 5×5(cm×cm) cut at 0.5GeV

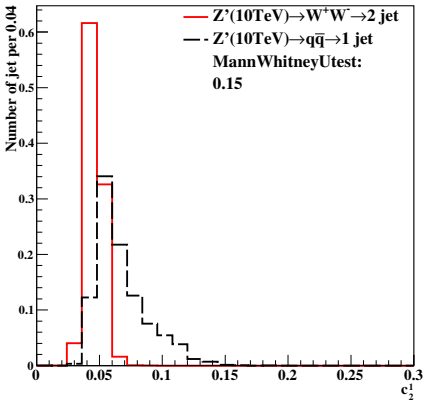

(d) 10TeV at 5×5(cm×cm) cut at 0.5GeV

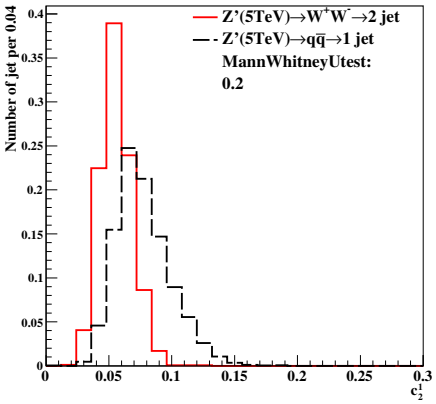

(e) 5TeV at 1×1(cm×cm) cut at 0.5GeV

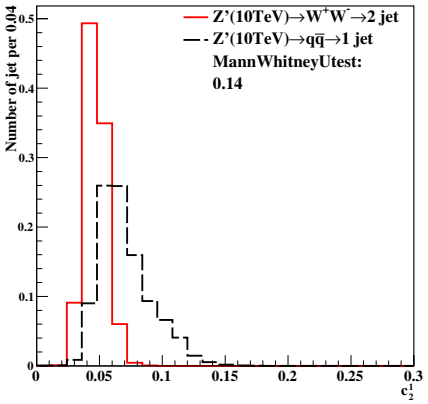

(f) 10TeV at 1×1(cm×cm) cut at 0.5GeV

Figure 7: Distributions of Mann-Whitney value U in 5,10TeV energy collision for $c_2^{(1)}$ in different detector sizes. Cell Size in 20×20, 5×5, and 1×1(cm×cm) are shown here.

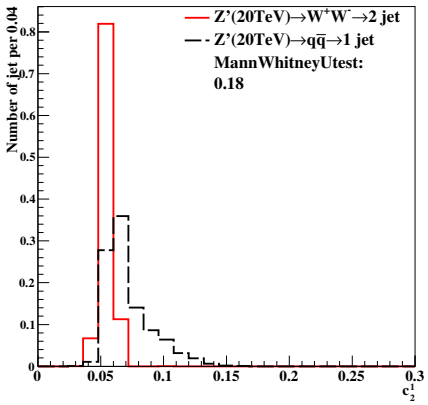

(a) 20TeV at 20×20(cm×cm) cut at 0.5GeV

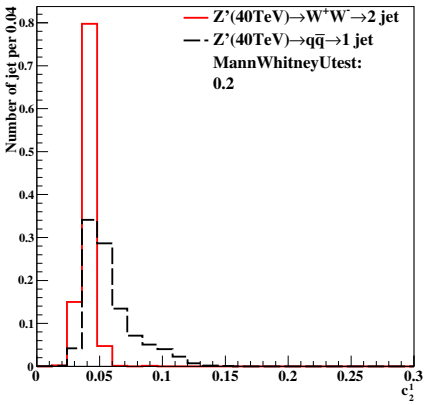

(b) 40TeV at 20×20(cm×cm) cut at 0.5GeV

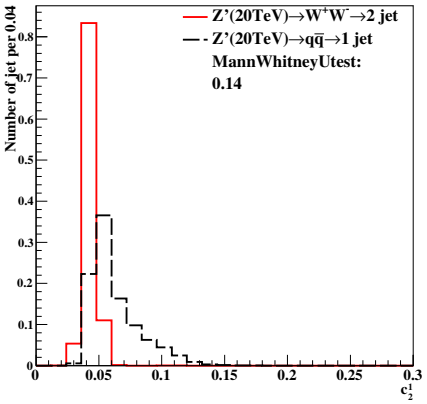

(c) 20TeV at 5×5(cm×cm) cut at 0.5GeV

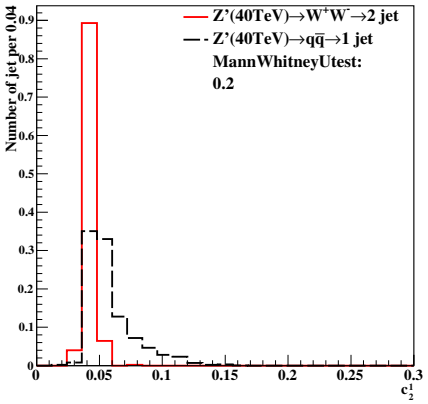

(d) 40TeV at 5×5(cm×cm) cut at 0.5GeV

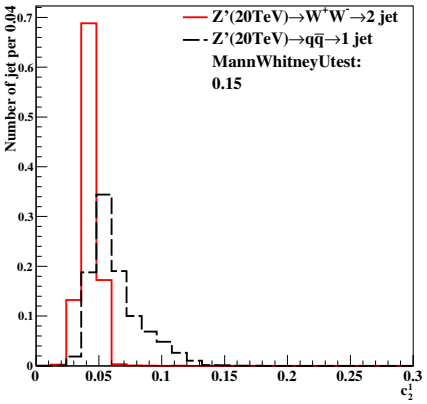

(e) 20TeV at 1×1(cm×cm) cut at 0.5GeV

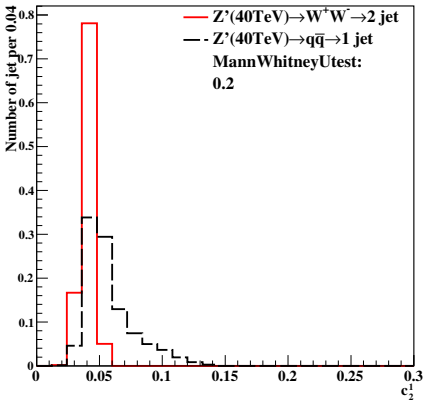

(f) 40TeV at 1×1(cm×cm) cut at 0.5GeV

Figure 8: Distributions of Mann-Whitney value U in 20,40TeV energy collision for $c_2^{(1)}$ in different detector sizes. Cell Size in 20×20, 5×5, and 1×1(cm×cm) are shown here.

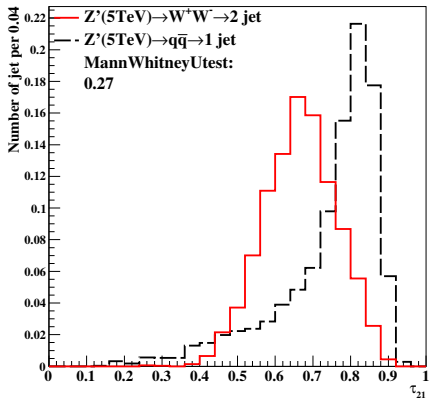

(a) 5TeV at 20×20(cm×cm) cut at 0.5GeV

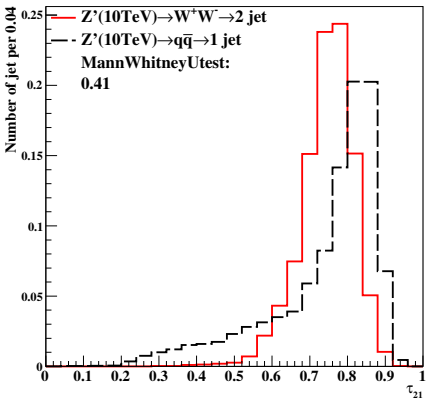

(b) 10TeV at 20×20(cm×cm) cut at 0.5GeV

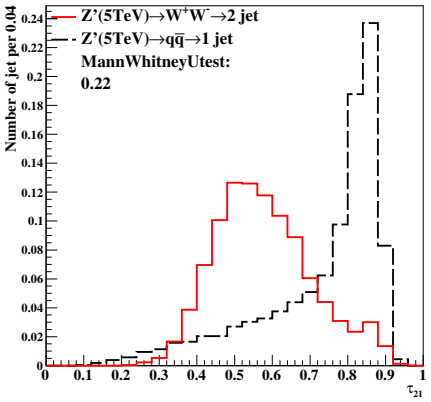

(c) 5TeV at 5×5(cm×cm) cut at 0.5GeV

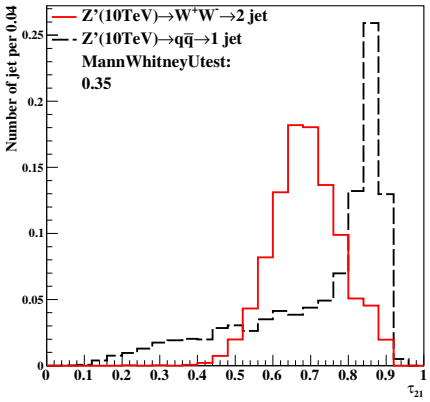

(d) 10TeV at 5×5(cm×cm) cut at 0.5GeV

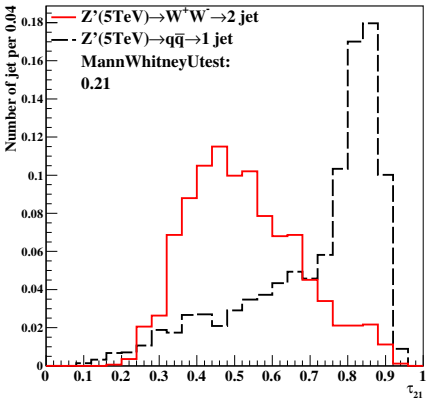

(e) 5TeV at 1×1(cm×cm) cut at 0.5GeV

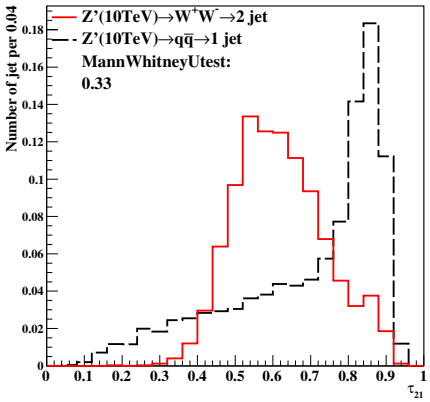

(f) 10TeV at 1×1(cm×cm) cut at 0.5GeV

Figure 9: Distributions of Mann-Whitney value U in 5,10TeV energy collision for τ_{21} in different detector sizes. Cell Size in 20×20, 5×5, and 1×1(cm×cm) are shown here.

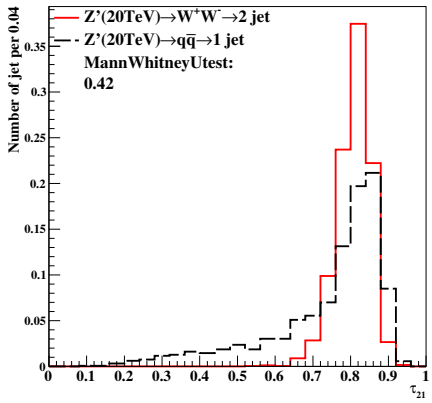

(a) 20TeV at 20×20(cm×cm) cut at 0.5GeV

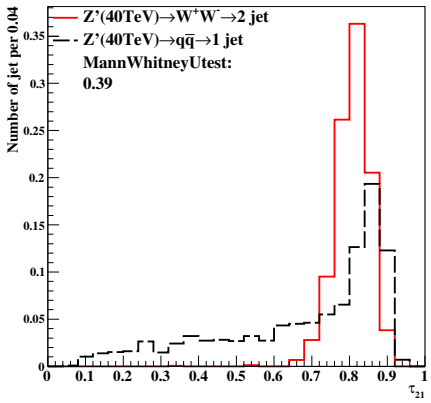

(b) 40TeV at 20×20(cm×cm) cut at 0.5GeV

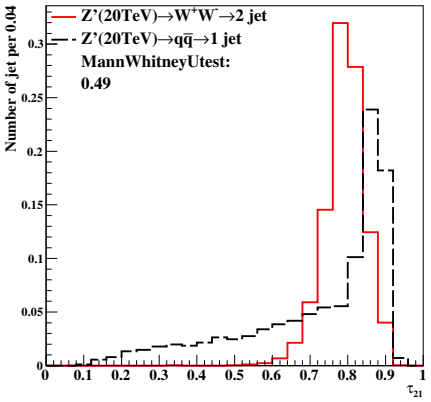

(c) 20TeV at 5×5(cm×cm) cut at 0.5GeV

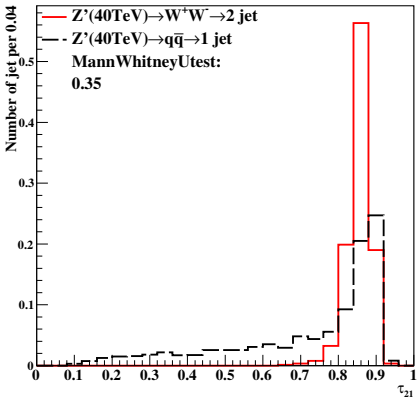

(d) 40TeV at 5×5(cm×cm) icut at 0.5GeV

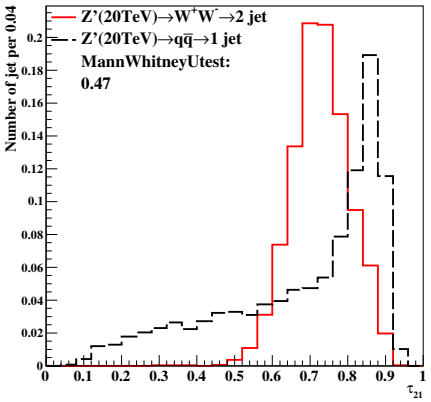

(e) 20TeV at 1×1(cm×cm) cut at 0.5GeV

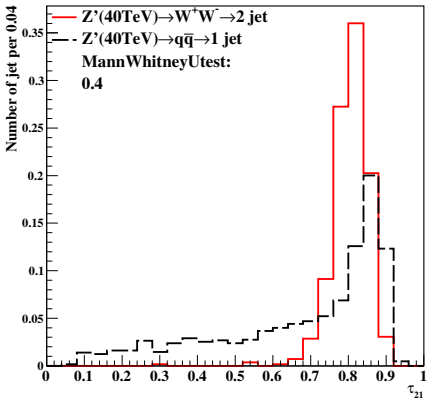

(f) 40TeV at 1×1(cm×cm) cut at 0.5GeV

Figure 10: Distributions of Mann-Whitney value U in 20,40TeV energy collision for τ_{21} in different detector sizes. Cell Size in 20×20, 5×5, and 1×1(cm×cm) are shown here.

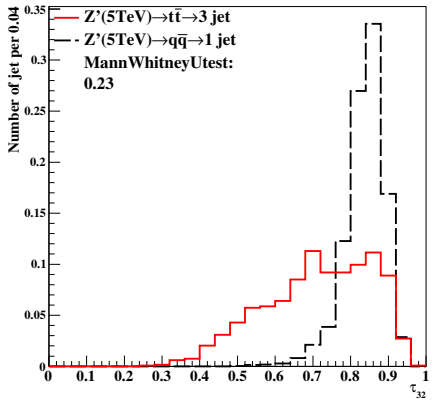

(a) 5TeV at 20×20(cm×cm) cut at 0.5GeV

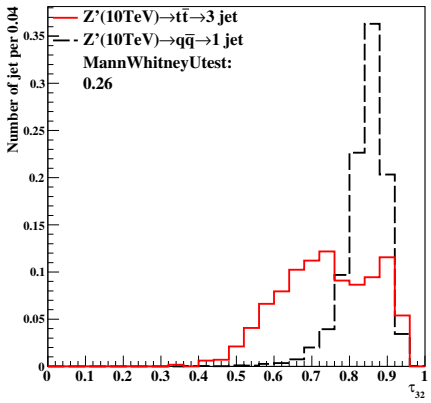

(b) 10TeV at 20×20(cm×cm) cut at 0.5GeV

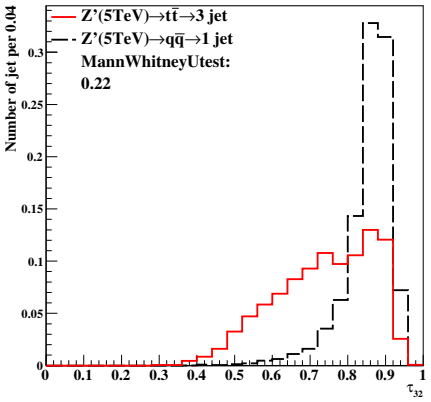

(c) 5TeV at 5×5(cm×cm) cut at 0.5GeV

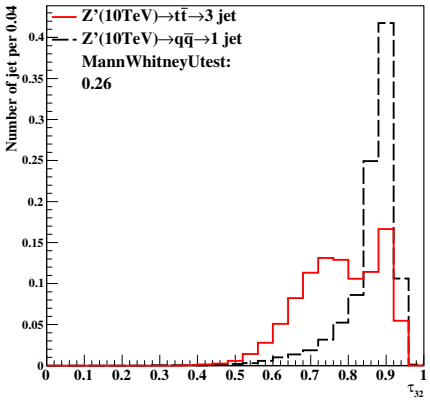

(d) 10TeV at 5×5(cm×cm) cut at 0.5GeV

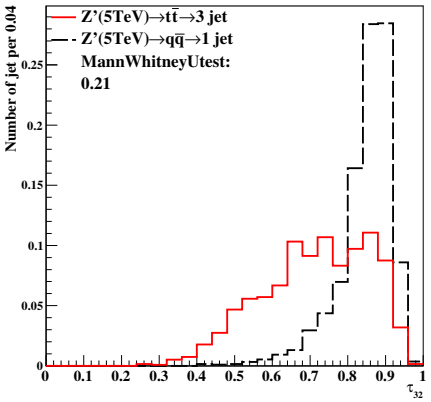

(e) 5TeV at 1×1(cm×cm) cut at 0.5GeV

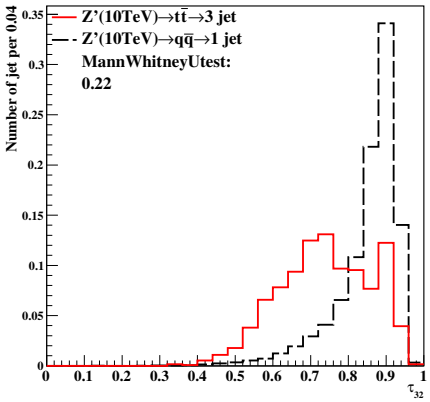

(f) 10TeV at 1×1(cm×cm) cut at 0.5GeV

Figure 11: Distributions of Mann-Whitney value U in 5,10TeV energy collision for τ_{32} in different detector sizes. Cell Size in 20×20, 5×5, and 1×1(cm×cm) are shown here.

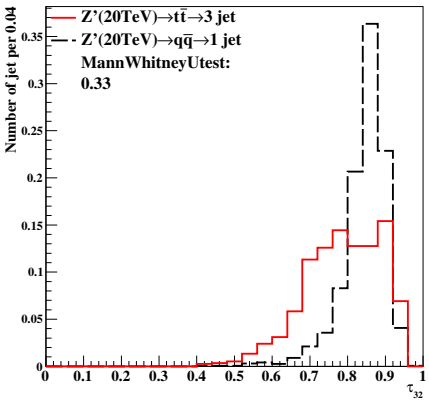

(a) 20TeV at 20×20(cm×cm) cut at 0.5GeV

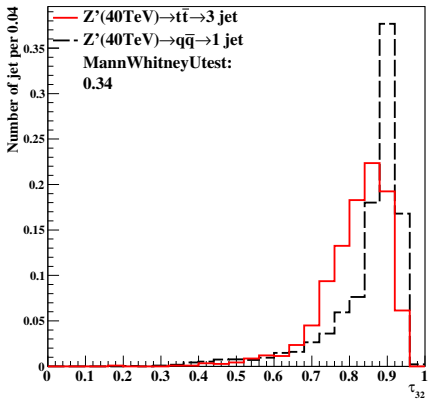

(b) 40TeV at 20×20(cm×cm) cut at 0.5GeV

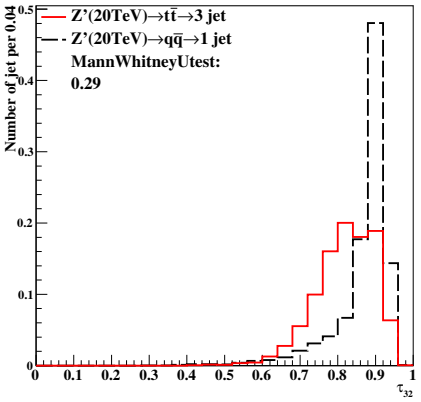

(c) 20TeV at 5×5(cm×cm) cut at 0.5GeV

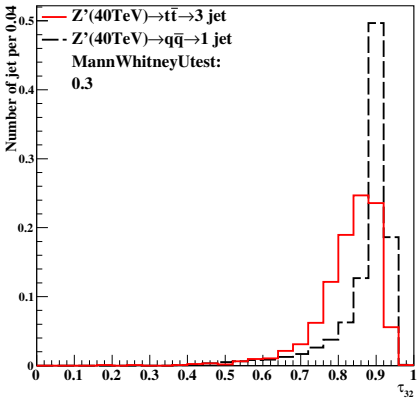

(d) 40TeV at 5×5(cm×cm) cut at 0.5GeV

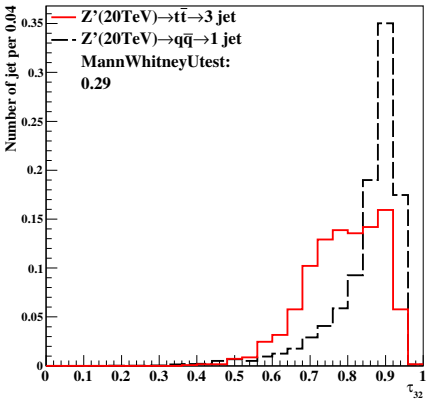

(e) 20TeV at 1×1(cm×cm) cut at 0.5GeV

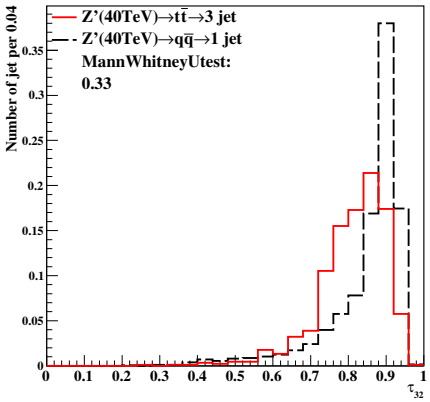

(f) 40TeV at 1×1(cm×cm) cut at 0.5GeV

Figure 12: Distributions of Mann-Whitney value U in 20,40TeV energy collision for τ_{32} in different detector sizes. Cell Size in 20×20, 5×5, and 1×1(cm×cm) are shown here.

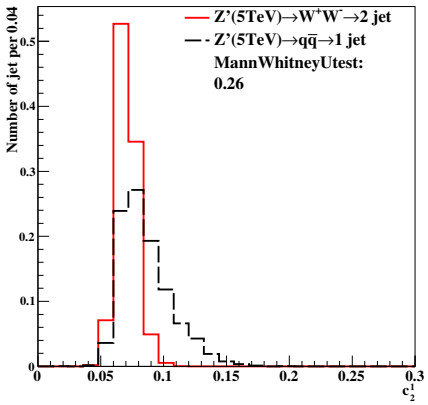

(a) 5TeV at 20×20(cm×cm) cut at 0.25GeV

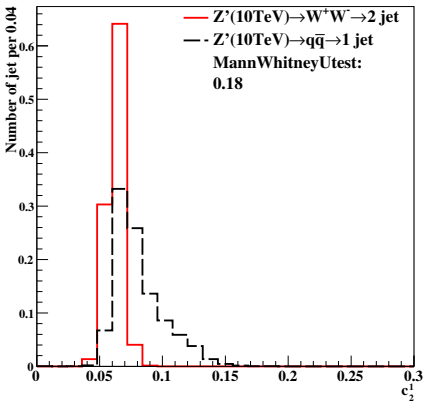

(b) 10TeV at 20×20(cm×cm) cut at 0.25GeV

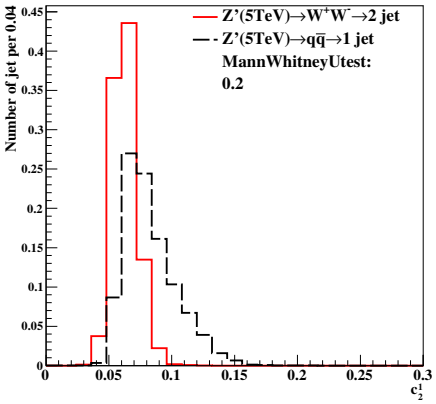

(c) 5TeV at 5×5(cm×cm) cut at 0.25GeV

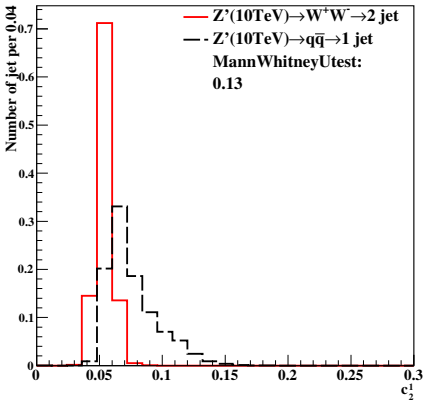

(d) 10TeV at 5×5(cm×cm) cut at 0.25GeV

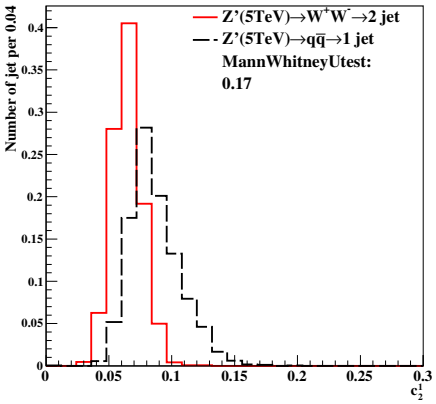

(e) 5TeV at 1×1(cm×cm) cut at 0.25GeV

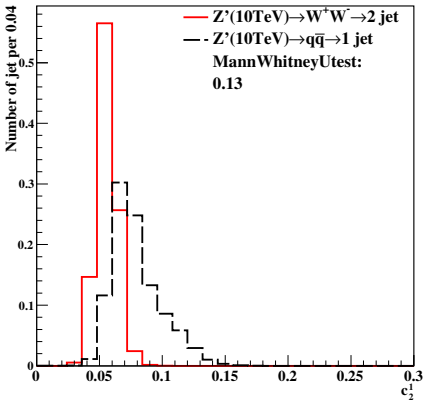

(f) 10TeV at 1×1(cm×cm) cut at 0.25GeV

Figure 13: Distributions of Mann-Whitney value U in 5,10TeV energy collision for $c_2^{(1)}$ in different detector sizes. Cell Size in 20×20, 5×5, and 1×1(cm×cm) are shown here.

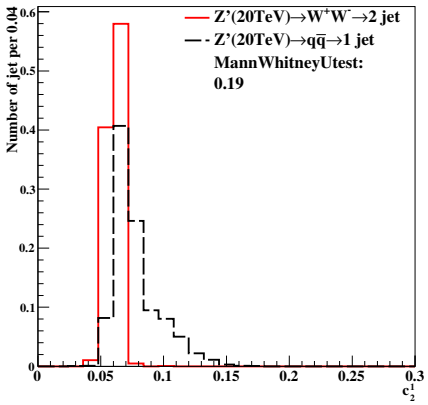

(a) 20TeV at 20×20(cm×cm) cut at 0.25GeV

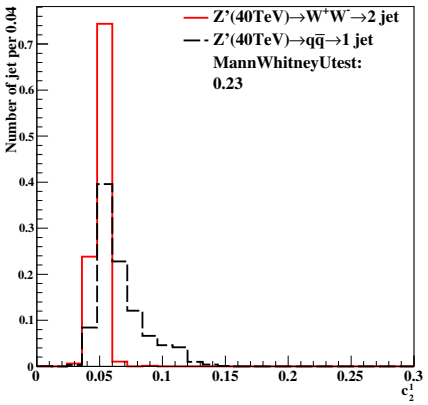

(b) 40TeV at 20×20(cm×cm) cut at 0.25GeV

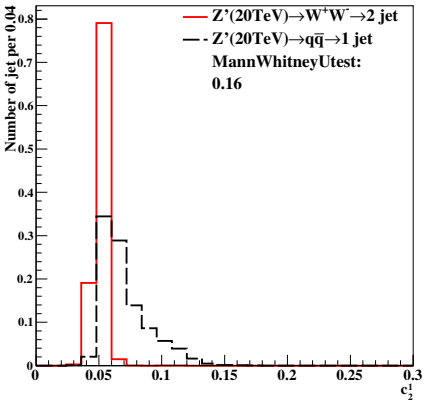

(c) 20TeV at 5×5(cm×cm) cut at 0.25GeV

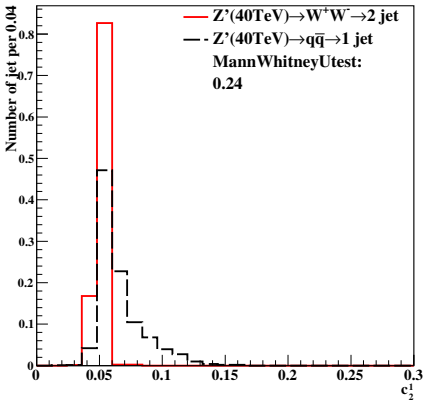

(d) 40TeV at 5×5(cm×cm) cut at 0.25GeV

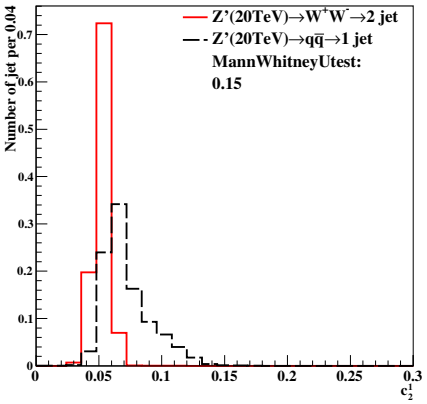

(e) 20TeV at 1×1(cm×cm) cut at 0.25GeV

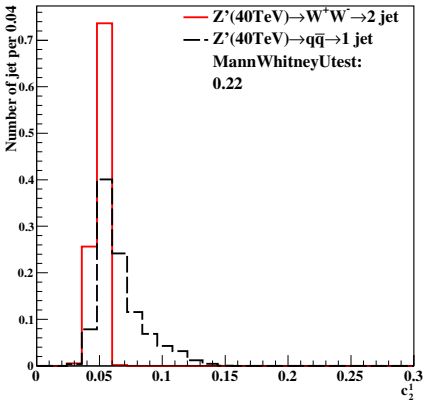

(f) 40TeV at 1×1(cm×cm) cut at 0.25GeV

Figure 14: Distributions of Mann-Whitney value U in 20,40TeV energy collision for $c_2^{(1)}$ in different detector sizes. Cell Size in 20×20, 5×5, and 1×1(cm×cm) are shown here.

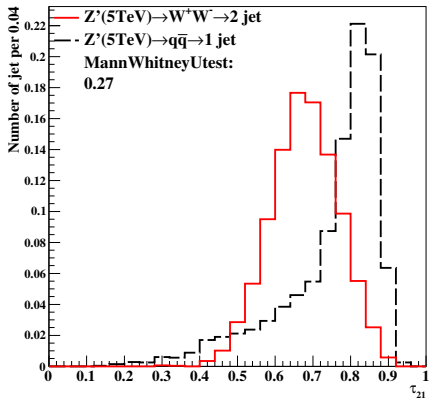

(a) 5TeV at 20×20(cm×cm) cut at 0.25GeV

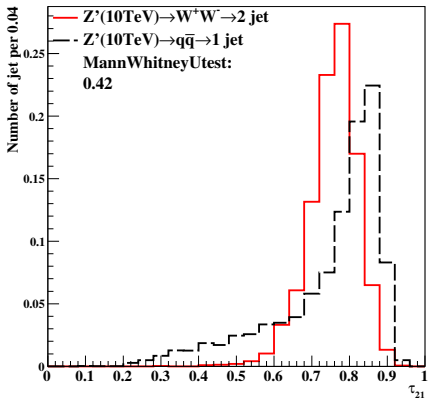

(b) 10TeV at 20×20(cm×cm) cut at 0.25GeV

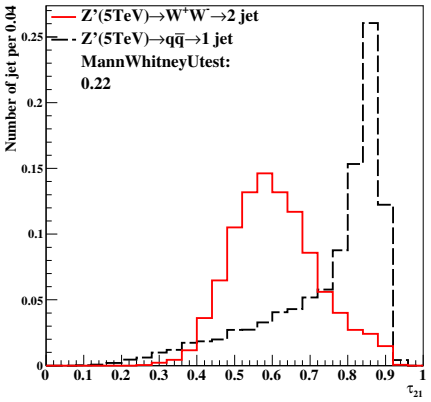

(c) 5TeV at 5×5(cm×cm) cut at 0.25GeV

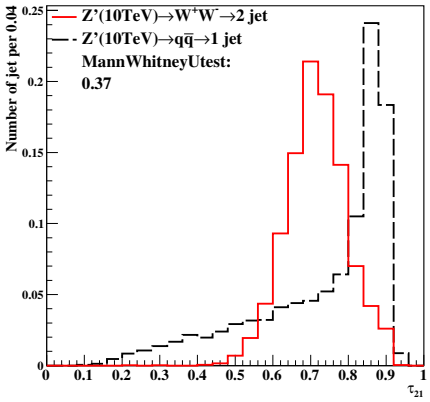

(d) 10TeV at 5×5(cm×cm) cut at 0.25GeV

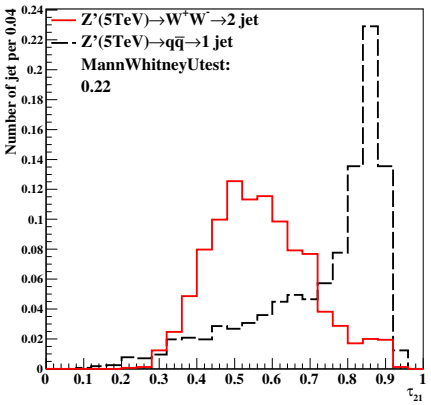

(e) 5TeV at 1×1(cm×cm) cut at 0.25GeV

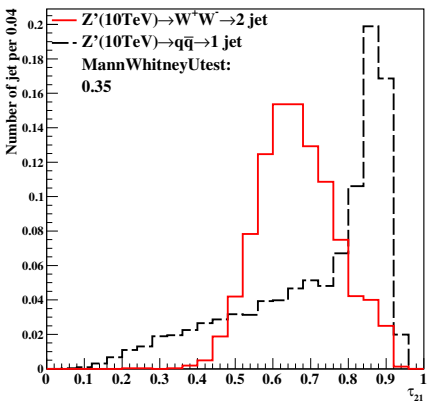

(f) 10TeV at 1×1(cm×cm) cut at 0.25GeV

Figure 15: Distributions of Mann-Whitney value U in 5,10TeV energy collision for τ_{21} in different detector sizes. Cell Size in 20×20, 5×5, and 1×1(cm×cm) are shown here.

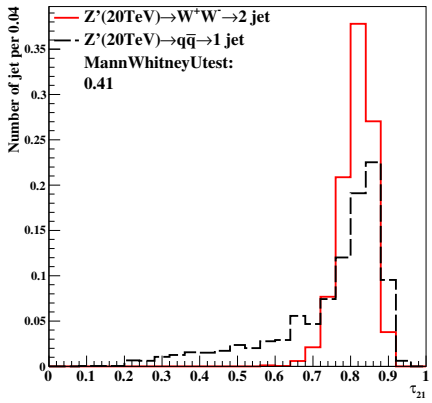

(a) 20TeV at 20×20(cm×cm) cut at 0.25GeV

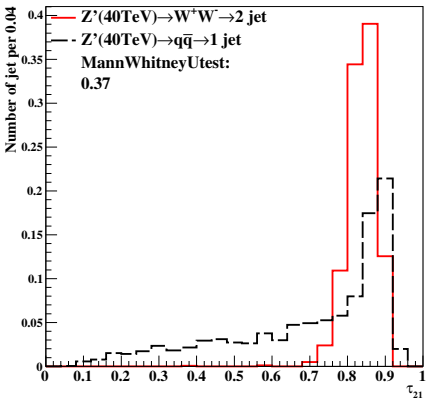

(b) 40TeV at 20×20(cm×cm) cut at 0.25GeV

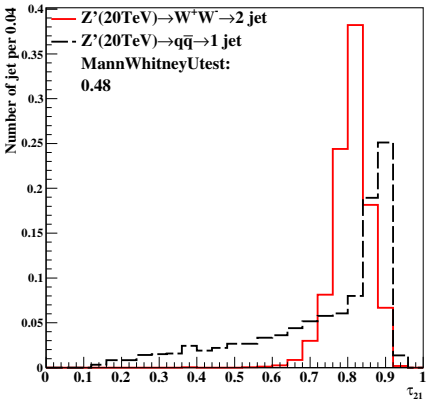

(c) 20TeV at 5×5(cm×cm) cut at 0.25GeV

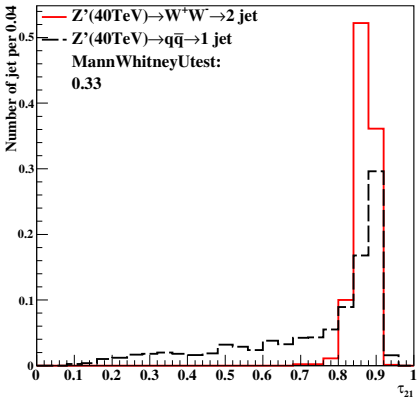

(d) 40TeV at 5×5(cm×cm) icut at 0.25GeV

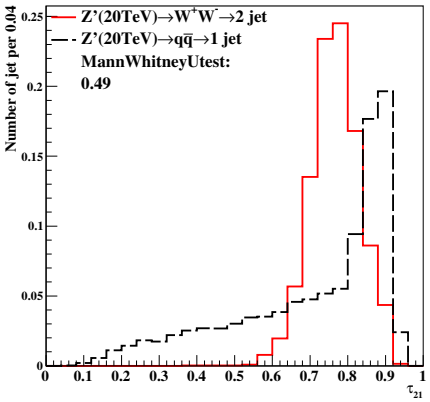

(e) 20TeV at 1×1(cm×cm) cut at 0.25GeV

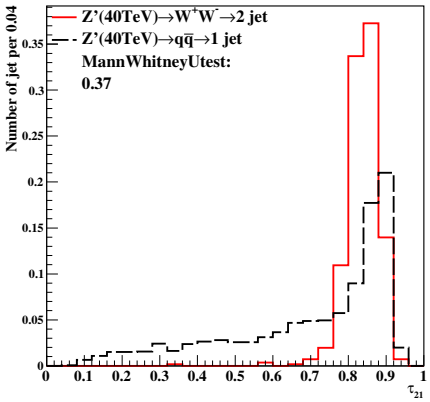

(f) 40TeV at 1×1(cm×cm) cut at 0.25GeV

Figure 16: Distributions of Mann-Whitney value U in 20,40TeV energy collision for τ_{21} in different detector sizes. Cell Size in 20×20, 5×5, and 1×1(cm×cm) are shown here.

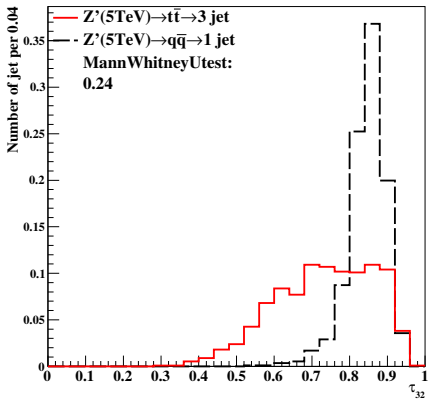

(a) 5TeV at 20×20(cm×cm) cut at 0.25GeV

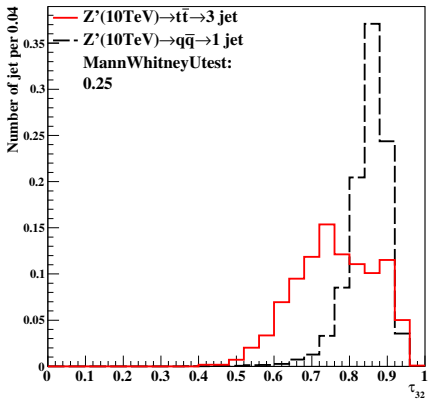

(b) 10TeV at 20×20(cm×cm) cut at 0.25GeV

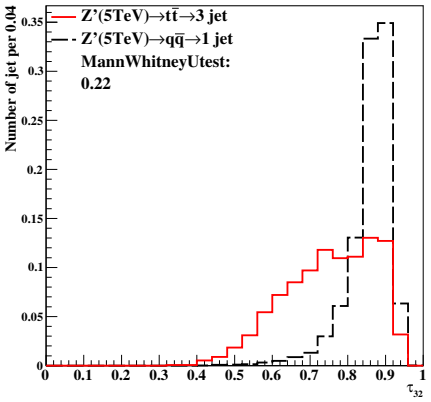

(c) 5TeV at 5×5(cm×cm) cut at 0.25GeV

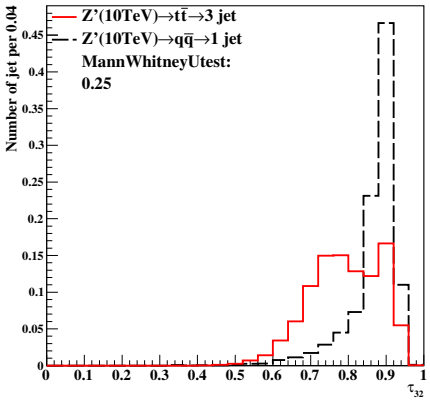

(d) 10TeV at 5×5(cm×cm) cut at 0.25GeV

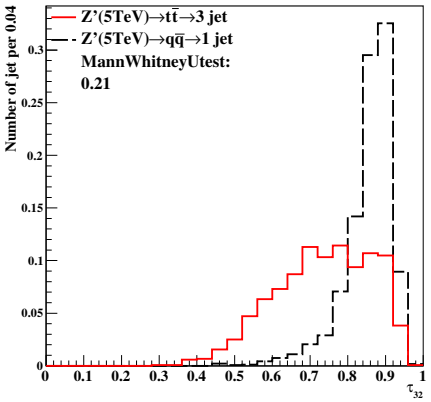

(e) 5TeV at 1×1(cm×cm) cut at 0.25GeV

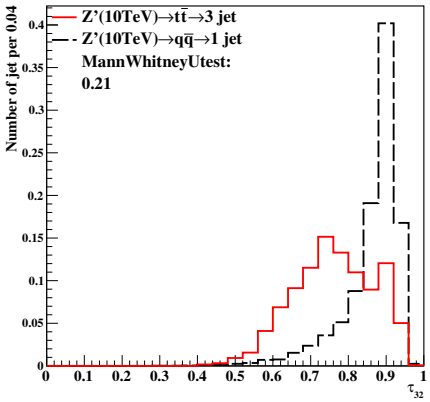

(f) 10TeV at 1×1(cm×cm) cut at 0.25GeV

Figure 17: Distributions of Mann-Whitney value U in 5,10TeV energy collision for τ_{32} in different detector sizes. Cell Size in 20×20, 5×5, and 1×1(cm×cm) are shown here.

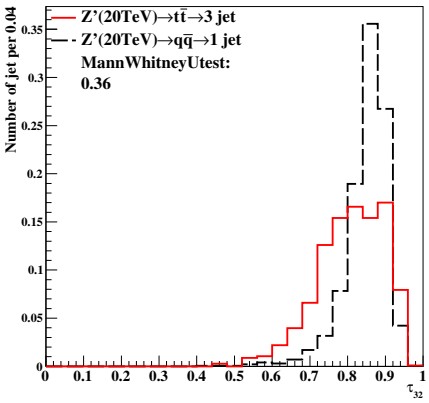

(a) 20TeV at 20×20(cm×cm) cut at 0.25GeV

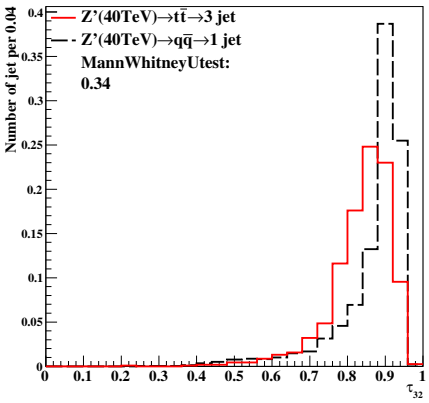

(b) 40TeV at 20×20(cm×cm) cut at 0.25GeV

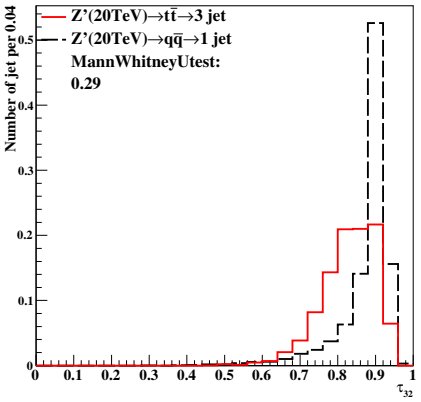

(c) 20TeV at 5×5(cm×cm) cut at 0.25GeV

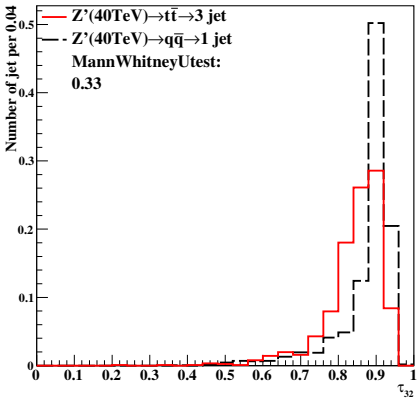

(d) 40TeV at 5×5(cm×cm) cut at 0.25GeV

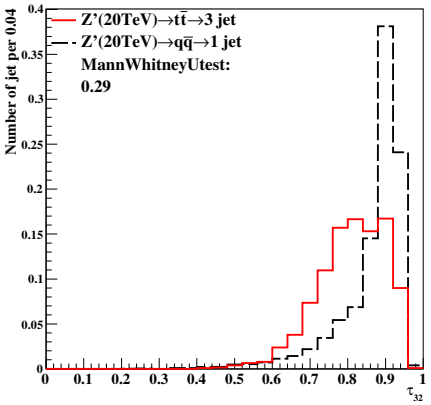

(e) 20TeV at 1×1(cm×cm) cut at 0.25GeV

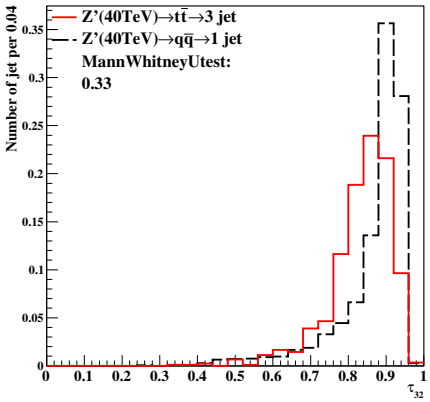

(f) 40TeV at 1×1(cm×cm) cut at 0.25GeV

Figure 18: Distributions of Mann-Whitney value U in 20,40TeV energy collision for τ_{32} in different detector sizes. Cell Size in 20×20, 5×5, and 1×1(cm×cm) are shown here.

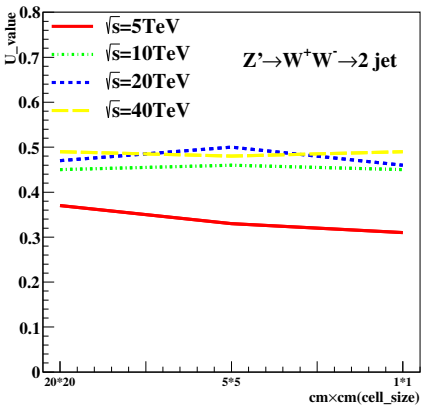

(a) τ_{21} in cluster

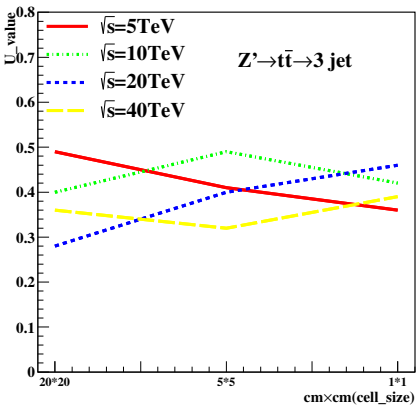

(b) τ_{32} in cluster

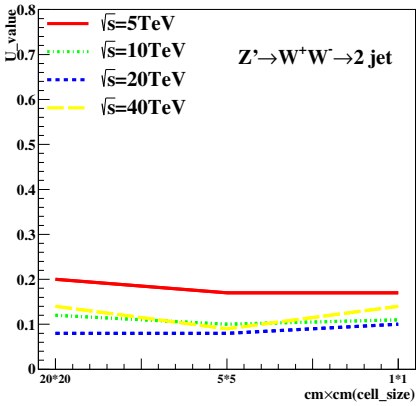

(c) $c_2^{(1)}$ in cluster

Figure 19: The Mann-Whitney U values for τ_{21},τ_{32} and $c_2^{(1)}$ reconstructed from calorimeter clusters at different collision energies correspond to different detector sizes in cluster. The energies of collision at 5, 10, 20, 40TeV are shown in each figure.

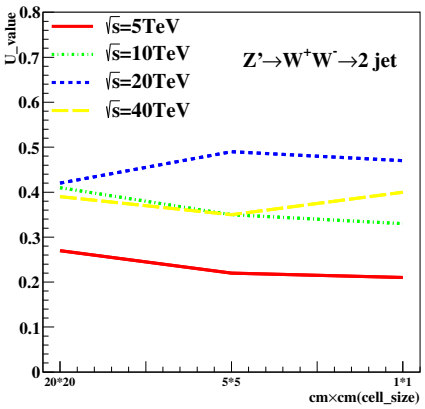

(a) τ_{21} rawhit cut at 0.5GeV

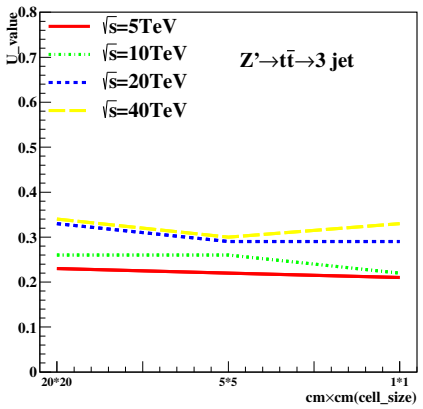

(b) τ_{32} rawhit cut at 0.5GeV

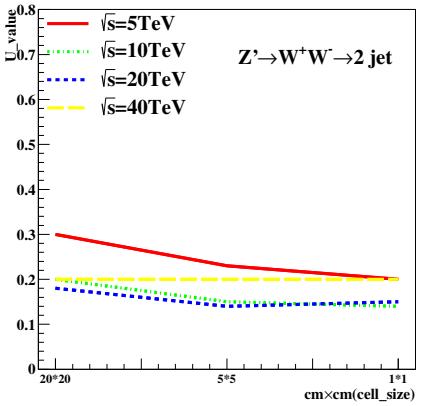

(c) $c_2^{(1)}$ rawhit cut at 0.5GeV

Figure 20: The Mann-Whitney U values for τ_{21},τ_{32} and $c_2^{(1)}$ reconstructed from calorimeter hit at 05GeV cut at different collision energies correspond to different detector sizes in rawhit cut at 05GeV. The energies of collision at 5, 10, 20, 40TeV are shown in each figure.

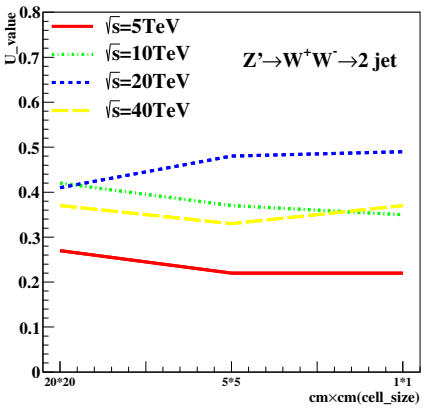

(a) τ_{21} rawhit cut at 0.25GeV

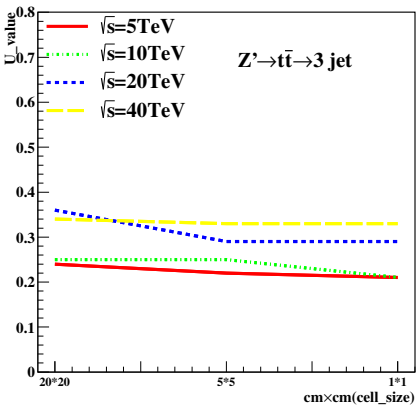

(b) τ_{32} rawhit cut at 0.25GeV

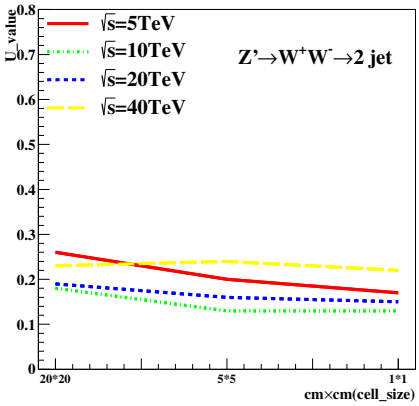

(c) $c_2^{(1)}$ rawhit cut at 0.25GeV

Figure 21: The Mann-Whitney U values for τ_{21},τ_{32} and $c_2^{(1)}$ reconstructed from calorimeter hit at 0.25GeV cut at different collision energies correspond to different detector sizes in cluster. The energies of collision at 5, 10, 20, 40TeV are shown in each figure.